

Effects of Salt on Phase Behavior and Rheological Properties of Alginate–Chitosan Polyelectrolyte Complexes

Anandavalli Varadarajan, Logan T. Kearney, Jong K. Keum, Amit K Naskar, and Santanu Kundu*



Cite This: *Biomacromolecules* 2023, 24, 2730–2740



Read Online

ACCESS |



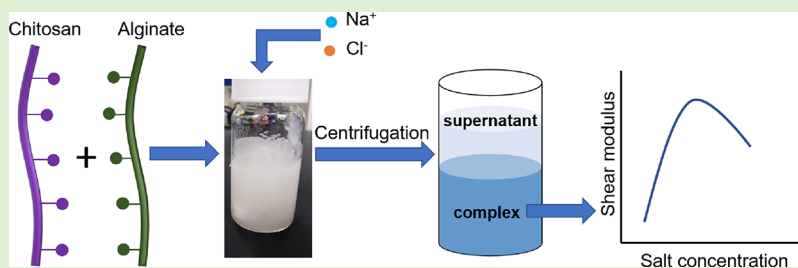
Metrics & More



Article Recommendations



Supporting Information



ABSTRACT: Oppositely charged polyelectrolytes often form polyelectrolyte complexes (PECs) due to the association through electrostatic interactions. Obtaining PECs using natural, biocompatible polyelectrolytes is of interest in the food, pharmaceutical, and biomedical industries. In this work, PECs were prepared from two biopolymers, positively charged chitosan and negatively charged alginate. We investigate the changes in the structure and properties of PECs by adding sodium chloride (salt doping) to the system. The shear modulus of PECs can be tuned from ~ 10 to 10^4 Pa by changing the salt concentration. The addition of salt led to a decrease in the water content of the complex phase with increasing shear modulus. However, at a very high salt concentration, the shear modulus of the complex phase decreased but did not lead to the liquid coacervate formation, typical of synthetic polyelectrolytes. This difference in phase behavior has likely been attributed to the hydrophobicity of chitosan and long semiflexible alginate and chitosan chains that restrict the conformational changes. Large amplitude oscillatory shear experiments captured nonlinear responses of PECs. The compositions of the PECs, determined as a function of salt concentration, signify the preferential partitioning of salt into the complex phase. Small-angle X-ray scattering of the salt-doped PECs indicates that the Kuhn length and radius of the alginate–chitosan associated structure qualitatively agree with the captured phase behavior and rheological data. This study provides insights into the structure–property as a function of salt concentration of natural polymer-based PECs necessary for developing functional materials from natural polyelectrolytes.

INTRODUCTION

Polyelectrolytes (PEs) are macromolecules having ionizable groups that can dissociate in aqueous solutions to form charged polymers and counterions.¹ After dissociation, these PEs gain unique properties such as water solubility, ionic conductivity, and the capability of developing ionic interactions with oppositely charged molecules.^{2–4} For example, ionic interactions with oppositely charged polymers can lead to the formation of polyelectrolyte complexes (PECs). Although PECs are increasingly being investigated for use in various fields such as biomedical, food products, underwater adhesives, and personal care products, the mechanism of complex formation and structure and properties of these complexes are still poorly understood.^{5,6}

In addition to the intrinsic polymer properties such as chemical structure, chain length, and charge ratio, the noncovalent interactions between polymer chains such as steric, van der Waals and hydrophobic interactions, and external environments such as pH, ionic strength of the media, and temperature dictate the structure and properties of the

complexes.^{5,7–9} PECs can either form one soluble/miscible phase or two phases, one rich and another dilute, for various combinations of polyelectrolytes.^{5,7,10} The dense phase can be either a viscous liquid with a high water content or a solid with less water content.^{9,11}

The phase behavior in these systems results from a complex interplay between factors such as polymer chemistry, chain length, polymer concentration, charge ratio, temperature, pH, and ionic strength.^{5,7,8,12} The alteration in ionic strength of the media caused by the addition of salts (salt doping) can also alter the phase behavior.^{13,14} It has been shown that increased salt concentration leads to phase transformation from solid precipitates to liquid coacervates and then to a homogeneous

Received: February 19, 2023

Revised: May 15, 2023

Published: June 1, 2023



solution.^{7,10,15} The mechanical responses of the complexes and their phase behavior with changing salt concentrations have been investigated by employing shear rheometry.^{7,8,13}

Most of the investigations on the phase behavior of PECs in the literature involve a limited selection of synthetic polyelectrolytes. In contrast, studies on the phase change of natural polyelectrolyte complexes with the addition of salt are limited.^{9,11–14,16,17} Natural polyelectrolytes with high molecular weight, stiffer backbones, and long-range ionic interactions are expected to behave differently than synthetic polyelectrolytes. The formation of PECs from biopolymer pairs can be seen in several living systems responsible for various biological functions.¹⁸ Examples include calcification of cartilage in mammals through salt-mediated complexation between cartilage lysozyme and proteoglycans,¹⁹ the antithrombic activity of heparin through electrostatic binding,²⁰ and complexation of proteins secreted by sandcastle worm, which is used to glue the exogenous mineral particles in their process to build protective shells.²¹ PECs formed from polysaccharide polyelectrolytes such as alginate, chitosan, pectin, xanthan gum, carrageenan, gum arabic, and hyaluronic acid have gained significant interest due to their nontoxicity and biocompatibility, making them suitable for biomedical applications and food products.^{2,5,22–27}

Herein, we utilized alginate, a natural anionic polysaccharide extracted from marine brown algae, and chitosan, the only natural cationic polysaccharide formed by *N*-deacetylation of chitin found in crustacean shells. Both alginate and chitosan are extensively studied biopolymers for different applications, including as model polysaccharides. They have been studied individually, as in solution and in gel form.^{28–32} Several studies have documented the complex formation between alginate and chitosan, particularly focusing on the effect of alginate/chitosan ratio, pH, and the order of addition, such as mixing alginate to chitosan, or vice versa.^{23,24,33} These complexes have been investigated for several applications in various forms, including beads, nanoparticles, and hydrogels for protein, drug, and cell encapsulation,^{23–25,34} and membranes for wound dressing.^{26,27} In limited studies, it has been shown that salt addition can affect the alginate–chitosan complex formations.^{35,36} For example, complexes obtained for a NaBr concentration of 1 M and subsequent ultracentrifugation resulted in a complex with a high storage modulus of $\sim 10^6$ Pa.³⁵

Controlled complexation caused by desalting through dialysis was utilized to obtain hydrogels and colloids from hyaluronic acid–chitosan, chitosan–heparin sodium salt, and chitosan–dextran sulfate.^{22,37,38} Porod law was used to fit the scattering data for these samples, and fitting for chitosan–heparin sodium salt and chitosan–dextran sulfate revealed rough fractal-like surfaces with the rod-like intra-particle structure captured by a slope of 3.8 in the low q range and 1 at the high q range, respectively.^{37,38} A similar structure was revealed for stretchable hydrogels obtained from hyaluronic acid and chitosan, where the semi-rough solid-like aggregates have sizes in the range of 100 nm to 1 μ m.²² For synthetic PEs, such as in the case of poly((vinylbenzyl)trimethylammonium chloride) (PVBtMA)–poly(styrenesulfonate) (PSS) system, the formation of clustered aggregates (solid phase) in the undoped state and rearrangement of that to a ladder-like structure (liquid phase) with doping (using NaBr) has been revealed.¹³

Here, we investigated the change in phase behavior and rheological properties of the PECs obtained from the alginate and chitosan upon salt doping using NaCl. We elucidated the mechanical behavior of the complex (polymer-rich) phase using small amplitude and large amplitude oscillatory shear (LAOS) measurements. Thermogravimetric analysis was utilized in measuring the water, salt, and polymer contents to probe the phase behavior. Small-angle X-ray scattering was used to understand the physical structure of the complex phase.

EXPERIMENTAL SECTION

Materials. The following materials were purchased from Sigma-Aldrich and used as received: sodium alginate (CAS # 9005-38-3), chitosan (CAS # 9012-76-4, low molecular weight), sodium chloride, potassium bromide, sodium bromide, and potassium iodide. Glacial acetic acid with a normality of 17.4 was used. DI water with a resistivity of 18.2 M Ω at 25 °C purified using a MilliporeSigma filtration system was used to prepare the stock solutions.

Preparation of Alginate and Chitosan Solutions. Alginate solutions (1% w/v) were prepared using DI water, and chitosan solutions (1% w/v) were prepared using 0.2 M acetic acid. The pH of the as-prepared alginate and chitosan solutions were ~ 6.5 and 4.0, respectively.

Molecular Weight Determination. The molecular weights of alginate and chitosan were determined from the intrinsic viscosity measured using a Ubbelohde viscometer (approximate constant: 0.03 cSt/sec, size-1C, viscosity range: 6 to 30 cSt). For molecular weight determination, sodium alginate and chitosan solutions were prepared in 0.1 M NaCl and 0.3 M acetic acid/0.2 M sodium acetate with concentrations in the range of 0.001 to 0.01 g/mL, respectively.

Degree of Deacetylation (DD). The degree of deacetylation of chitosan was determined using IR spectroscopy. The analysis was carried out for the as-received chitosan powder in a PerkinElmer Spectrum Two spectrometer. A total of 256 scans were collected over the range of 550 to 4000 cm^{-1} with a resolution of 4 cm^{-1} .

Preparation of Polyelectrolyte Complexes (PECs). To obtain PECs, chitosan solution was added dropwise to the alginate solution until 1:1 volume ratio was obtained. The solution was stirred using a mechanical stirrer at ≈ 700 rpm until the mixture changed to an opaque colloid. The samples were stored in the refrigerator at ≈ 4 °C prior to conducting characterizations. To dope the PECs with salts, NaCl was added gradually in powder form until the desired molarity was attained. The sample was then mixed with a glass stirrer until the salt dissolved completely.

Thermogravimetric Analysis. PEC samples with different salt concentrations were centrifuged in 1.5 mL Eppendorf tubes at 10,000 rpm for 15 min. The supernatant and complex phases were separated by pipetting out the supernatant. Around 30–40 mg of supernatant and complex was transferred to separate aluminum pans. The samples were then placed in an oven at 110 °C for 2.5 h to remove water. The corresponding weight loss was measured. Next, the pans were placed in a muffle furnace at 600 °C for 12 h in an inert nitrogen environment to remove the remaining water and to decompose the organic components, alginate, and chitosan. The weight loss for this process was measured. Three samples were gravimetrically measured for each salt concentration.

Rheology. For rheological measurements, samples were prepared at the required salt concentration and were centrifuged at 4000 rpm for 15–30 min. The complex phase was carefully separated using a disposable pipette and was used for rheological experiments. The experiments were performed using a stress-controlled rheometer, DHR-2 (TA Instruments), at 22 °C, precisely controlled by a Peltier system. A 20 mm parallel-plate geometry with solvent trap attachment filled with water was used to prevent drying of the sample during the rheological testing. Adhesive-backed sandpapers (grit number # 600, Allied High-Tech Products Inc.) were attached to both upper and lower plates to minimize sample slippage at the sample–rheometer

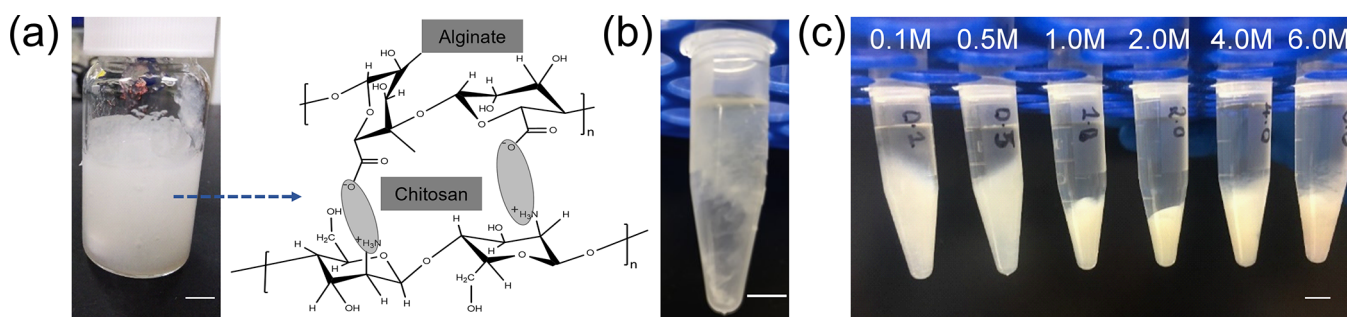


Figure 1. Images of the (a) as-prepared undoped PEC from alginate and chitosan solutions (concentration, 1% w/v) mixed in 1:1 volume ratio (the possible complexation between alginate and chitosan chains is shown); (b) undoped PEC after centrifugation; and (c) NaCl-doped PECs showing two-phase separation after centrifugation. The salt concentration in molarity for each case is shown. The scale bar represents 5 mm.

plate interface. Experiments were performed with a gap of 1000 μm . LAOS experiments were conducted for the strain amplitude range of 0.05–50% at a constant oscillation frequency of 1 Hz. Three sampling cycles were used, and the average of these three cycles is shown in our results. We have used the framework developed by Ewoldt et al.³⁹ to analyze the Lissajous plots. The stress response can be represented using Chebyshev polynomials of the first kind as

$$\tau(t) = \gamma_0 \sum_{n:\text{odd}} e_n T_n(x) + \dot{\gamma}_0 \sum_{n:\text{odd}} \nu_n T_n(y)$$

where $T_n(x)$ and $T_n(y)$ are the n th order Chebyshev polynomials of the first kind, $\dot{\gamma}_0$ is the strain rate amplitude, $x = \frac{\gamma}{\gamma_0}$, $y = \frac{\dot{\gamma}}{\dot{\gamma}_0}$, and e_n and ν_n are the elastic and viscous Chebyshev coefficients, respectively. MITlaos software has implemented this framework and was used to estimate the Chebyshev coefficients.

Small-Angle X-ray Scattering. SAXS measurements were collected on a Xeuss 3.0 (Xenocs, France) equipped with a D2+ MetalJet X-ray source (Ga $K\alpha$, 9.2 keV, $\lambda = 1.3414 \text{ \AA}$). PECs were loaded into 2 mm quartz capillaries, sealed, aligned perpendicular to the direction of the X-ray beam (transmission mode), and measured for 10 min at a sample-to-detector distance of 900 mm. 2D images of the scattering patterns were collected on a Eiger 2R 4 M hybrid photon counting detector with a pixel dimension of $75 \times 75 \mu\text{m}^2$ (Dectris, Switzerland). The 2D SAXS images were circularly averaged and reduced in the form of absolute intensity versus scattering vector (q), where $q = (4\pi \sin \theta)/\lambda$. Direct beam intensity was used to calibrate the measured intensities of each sample following background subtraction, and transmission corrections were applied in the XSACT software package (Xenocs, France). Multiple exposures greater than 20 min on the same sample area showed no effects of radiation damage. Data analysis and fitting were performed using Igor Pro and the analysis packages available through NIST Center for Neutron Research. Modeling of the PEC structure was performed using either the double power law or worm-like chain (flexible cylinder) models available in IgorPro environment.

RESULTS AND DISCUSSION

Molecular Weight Determination. The molecular weights of alginate and chitosan used here were estimated from the intrinsic viscosity values using Mark–Houwink equation, $[\eta] = k M^a$. Here, $[\eta]$ is the intrinsic viscosity in mL/g, M is the molecular weight in g/mol, and k and a are constants specific for a particular polymer–solvent system. The a and k for alginate are 0.97 and 0.002, respectively.^{30,40} Similarly, a and k values for chitosan are 0.76 and 0.074, respectively.^{31,41} Kraemer plots capturing inherent viscosity as a function of polymer concentration are shown in Figure S1 (Supporting Information), and the estimation of M is shown in Table S1. The estimated molecular weight of alginate and chitosan are ≈ 230 and 260

kg/mol, respectively. We calculated the number of charges considering full charge dissociation and alginate and chitosan molecular weight and their concentrations of 1% w/v as $\approx 2.8 \times 10^9/\text{mL}$ and $3.6 \times 10^9/\text{mL}$, respectively. The positive charges (in chitosan) was slightly higher than the negative charges (in alginate) but not significantly different. However, as shown below, such a minor difference has likely affected the phase behavior.

Degree of Deacetylation (DD). Chitin is hydrophobic and can be made water-soluble by deacetylation of *N*-acetyl glucosamine group present in the chain.⁴² The degree of DD was estimated using FTIR data as $\%DD = \left(\frac{A_{1655}}{A_{3450}} \right) \times \left(\frac{100}{1.33} \right)$ (Figure S2, Supporting Information).^{43,44} The intensity of the 1655 band, A_{1655} , is a measure of *N*-acetyl or amine content. The intensity of a 3450 band, A_{3450} , is a measure of the –OH stretching, which is the reference band that does not change with deacetylation. The A_{1655}/A_{3450} ratio is equal to 1.33 for fully *N*-acetylated chitin.⁴⁴ The %DD for the as-received chitosan sample was $\approx 82\%$.

Polyelectrolyte Complex Formation and Their Morphology. Alginate and chitosan with a concentration of 1% w/v were mixed in a 1:1 volume ratio using an overhead mixer until the mixture became opaque, indicating the complexation between alginate and chitosan. The mixture was stored overnight at 4 $^\circ\text{C}$ to ensure the completion of the process. The samples appeared to have a colloidal structure with no distinct phase separation (Figure 1a).

The images of the samples after centrifugation without and with salt addition (salt-doped) are shown in Figure 1b,c. Samples without salt did not show a clear phase separation with centrifugation (Figure 1b). However, for the salt-doped samples, the centrifugation led to clear phase separation, forming distinct solid (polyelectrolyte complex or PEC phase) and liquid (supernatant) phases (Figure 1b). The PEC phase appeared to be denser with increasing salt concentration (c) up to 2.0 M. However, the PECs for c equal to 4.0 and 6.0 M became less dense. Note that for this study, the maximum salt concentration considered was 6.0 M, slightly lower than the solubility limit of NaCl in water at the room temperature of 6.15 M.

In general, many synthetic cationic and anionic polyelectrolytes display two-phase separation (solid–liquid) on mixing and centrifugation.^{7,10,13,17} Here, the solid phase is the polymer-rich phase, and the liquid phase is the polymer-lean supernatant phase. The complex formation and phase separation are consistent among different synthetic systems, and the complexes obtained from them have some similarities

to that observed here. For example, a soft and white flowing particulate system was observed with PECs from PVBtMA and PSS.¹³ However, the complex obtained from PSS and poly(diallyldimethylammonium) (PDADMA) showed dense glassy solids.¹⁰ In both of these systems, the addition of salt resulted in a transition where the solid polymer-rich phase became the liquid phase (coacervate formation), resulting in liquid–liquid phase separation. This is caused by the dissolution of the complex due to the weaker attractive interactions between polyelectrolytes at high salt concentrations.^{7,10,13,17} But, liquid–liquid phase separation was not observed in our systems for the maximum salt concentration considered, and the complex phase was not glassy. However, our results are similar to the literature report of solid phase formation obtained after ultracentrifugation of alginate and chitosan mixtures.³⁵

Figure 2 shows a schematic of the proposed mechanism involved in the complexation of alginate and chitosan in the

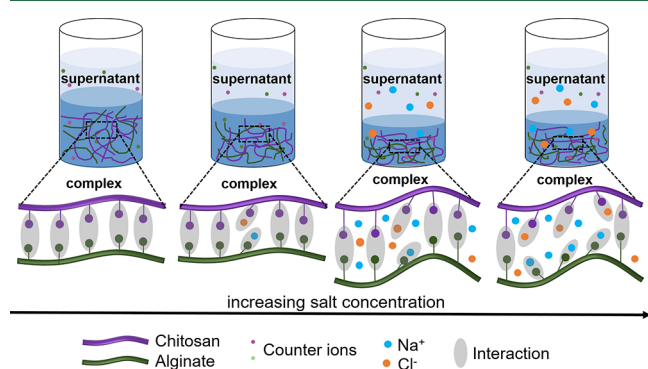


Figure 2. Schematic capturing the interactions involved in polyelectrolyte complexation of alginate and chitosan chains with increasing salt concentration.

presence of salt. The ionic interactions between the positively charged chitosan (Pol^+) and negatively charged alginate chains (Pol^-) result in a self-assembled structure, PECs. It has been hypothesized that when salt is added to the system, the charges are screened, which can cause the change from intrinsic (Pol^+ and Pol^-) to extrinsic (charged polymer and counterions from salt) ion pairs. At low salt concentrations, fewer intrinsic ion pairs are substituted, and with an increase in salt concentration, water is released because of osmotic pressure, causing the

denser complex phase.¹³ After a certain threshold in the salt concentration, more intrinsic pairs are substituted for the extrinsic pairs, associations are loosened, and the polyelectrolytes possibly rearrange to form loose ladder-like structures.¹³ Centrifugation of these salt-doped samples leads to phase separation, forming polymer-rich (complex) and polymer-lean (supernatant) phases.

Binodal Phase Diagram. The amounts of water, polymer, and salt in the complex and the supernatant phases were determined by using TGA. The water content in the complex phase for various salt concentrations is shown in Figure 3a. The water content without salt doping was ~ 98 wt %, which decreased (i.e., an increase in polymer concentration) with increased c up to 4.0 M. However, the water/polymer content did not change significantly beyond that. The water content was ~ 70 wt % for $c = 6.0$ M.

Figure 3b displays the binodal phase diagram obtained from the salt and polymer content in the complex and supernatant phase using TGA. As discussed above, PECs in the undoped sample could not be separated well into complex and supernatant phases (Figure 1a), resulting in a similar amount of polymer concentration in both the complex and supernatant phases. The polymer concentration in the complex phase increased with increasing salt concentration until it reached $c = 2.0$ M; however, it then decreased with increasing c . The polymer concentration in the complex phase was higher than in the supernatant phase for all cases. The increase in polymer concentration in the complex phase for up to 2 M salt addition can be attributed to a dehydration behavior caused by the external osmotic pressure upon salt doping. This behavior is similar to the poly-(diallyldimethylammonium)–PSS system and PVBtMA–PSS systems doped with NaCl and NaBr.^{13,45}

The polymer concentration in the PEC phase for $c = 4$ and 6 M salt doping decreased, resulting in a smaller difference in polymer concentration in the complex and supernatant phases. We hypothesize that an excessive salt concentration in the PEC led to the rupture of ion pairing between oppositely charged polyelectrolytes (formation of extrinsic ion pairs), causing the decreased polymer concentration in the complex phase. Since the behavior of polyelectrolytes is dependent on environmental pH, we measured the pH of the supernatants and found that the pH was almost similar for all cases.

The absence of transition from solid–liquid to liquid–liquid phase separation in our system can be attributed to several reasons. The longer and semiflexible chains of the alginate and

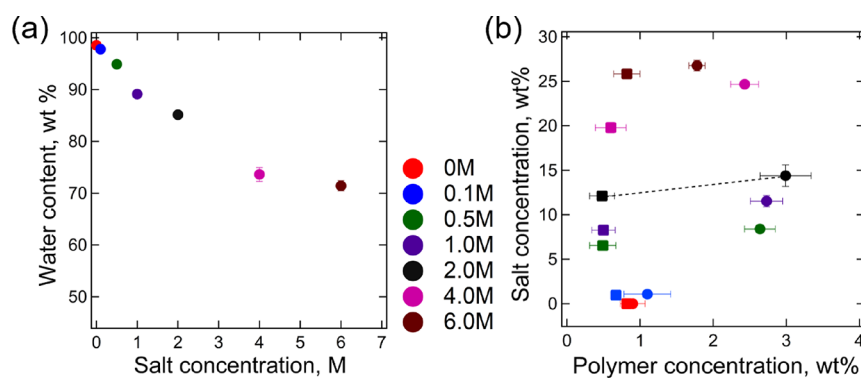


Figure 3. (a) Water content in the complex phase as a function of salt concentration (M). (b) Binodal phase behavior as a function of polymer and salt concentrations (wt %). The square symbols represent the supernatant phase, and the circles represent the complex phase. The dotted line is a representative tie-line. Error bars denote the standard deviation of three measurements.

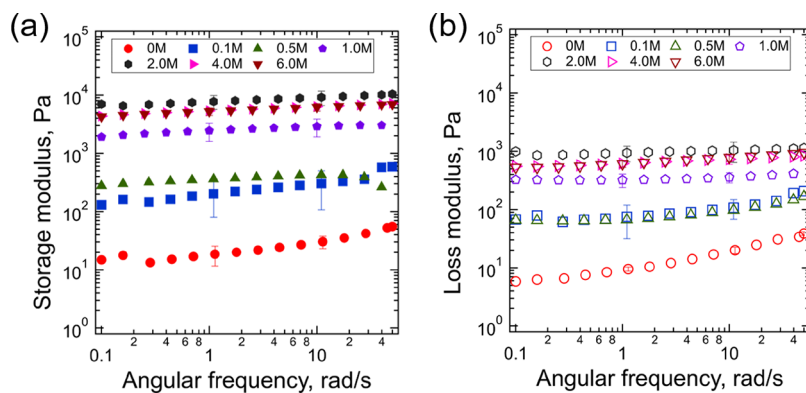


Figure 4. Frequency sweep results for PECs doped with different concentrations of NaCl. (a) Storage modulus (G') vs frequency and (b) loss modulus (G'') vs frequency. The applied strain amplitude was 1%.

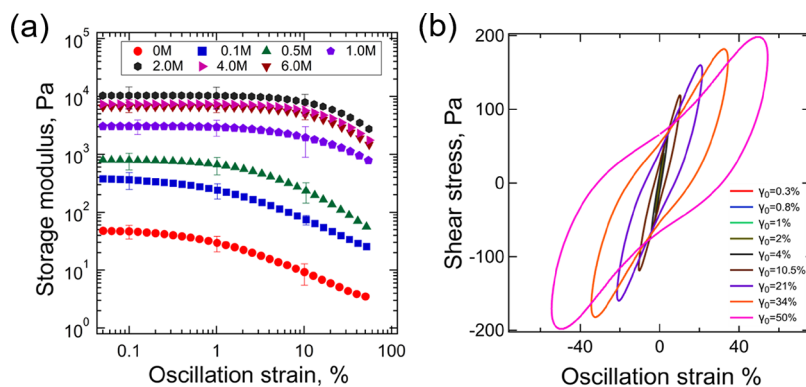


Figure 5. (a) G' as a function of oscillatory strain for PECs doped with different concentrations of NaCl and (b) Lissajous curves as a function of strain for a sample with 1.0 M NaCl. Here, the applied frequency was 1 Hz, and the Lissajous–Bowditch curves are an average of three cycles.

chitosan can resist the conformational change of the polymers.^{46–48} We also hypothesize that the sodium alginate chains are less susceptible to structural changes with the addition of NaCl as the polymer is already under the influence of Na⁺ ions.^{49,50} In a previous study, it has been shown using isothermal titration calorimetry that the addition of NaCl does not significantly affect the change of enthalpy of binding.⁴⁹ Further, the slight hydrophobic nature of the chitosan chain can also play a role, as it reduces the hydration level.^{46,47} A previous work from Schlenoff and co-workers has shown that the association between the polyelectrolytes in solid PECs is stronger with increasing hydrophobicity in the system.⁵¹ Specifically, the complexes obtained from poly(allylamine hydrochloride) and poly(acrylic acid sodium salt) did not show complete dissolution even at the maximum solubility concentration (6 M) of NaCl due to the hydrophobicity of the PEs.^{11,12,46} All these factors, in addition to the osmotic effect, control the phase behavior of our system.^{52,53} Correspondingly, Figure 1 and the characterization of PECs discussed below capture the change in structure and properties with changing NaCl concentration.

A partitioning of salt in the complex phase was observed, as shown by a positive tie line (Figure 3b). This behavior matches with the predictions shown by the Voorn–Overbeek (VO) model.⁵⁴ According to this model, increased polymer concentration with unbalanced charges in the complex phase can attract more salt ions to the complex phase. For our system, the number of positive and negative charges calculated based on molecular weight were slightly different from each other, and the extra charges available after complexation can

possibly attract additional counterions, leading to the partitioning of salt to the complex phase.

Further, we have extended our study by doping with different salts such as KBr, KI, and NaBr. These were conducted near the solubility limits of those salts. The complex phase formation appeared to be similar to that of NaCl. Particularly, adding salts did not cause liquid–liquid phase separation or a homogeneous solution of PECs (Figure S3). For many PEs, the efficiency of doping and critical salt concentration leading to a transition from solid–liquid to liquid–liquid phase has shown to be dependent on the type of salt ion, which usually follow the Hofmeister series.^{12,55–58} The absence of such behavior in our system needs additional investigations.

Rheological Properties. Rheological experiments were performed on the complex phase to demonstrate the change in mechanical properties with the addition of salt and the corresponding change in the water content. Figure 4 displays the storage (G') and loss moduli (G'') as a function of frequency obtained at a constant strain of 1% for different salt concentrations. Both G' and G'' increased with increasing c values up to 4.0 M, and then it decreased. The samples showed a very weak frequency dependence as both the moduli increased slightly with the increase in frequency. The storage modulus for the undoped sample was ~ 10 Pa, which increased significantly to $\sim 10^4$ Pa with increasing c to 2.0 M. A further increase in c resulted in a decrease in the modulus of the complex phase, but the magnitude was still in the order of 10^3 Pa. Here, $\tan \delta < 1$ at any salt concentration for the entire measured frequency range (Figure S4), signifying a solid-like

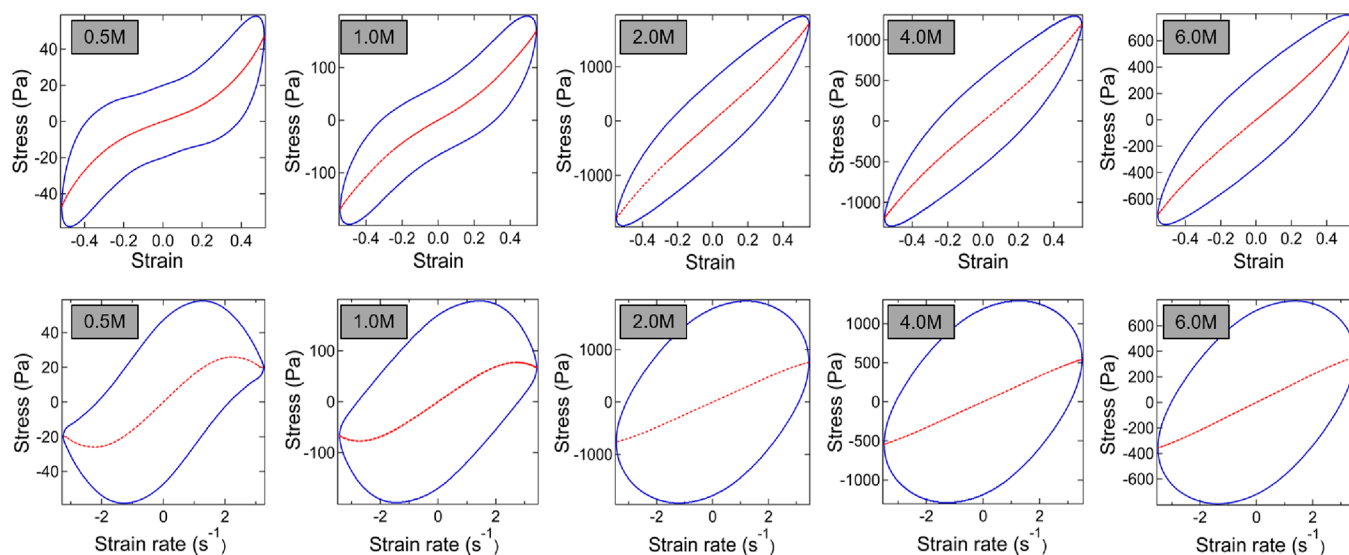


Figure 6. Top: Elastic Lissajous curves of stress vs strain at 50% strain for different salt concentrations. Bottom: Viscous Lissajous curves of stress vs strain rate at 50% strain; solid lines represent the total stress, and dashed lines represent the elastic and viscous stress.

behavior.⁵⁹ The samples did not show any cross-over from a solid to liquid behavior with the addition of salt, as mentioned in previous studies for the polyelectrolyte complexes formed from PSS–PDADMAC and PSS–PVBtMA.^{7,13} Further, Afzal et al. have shown that for pH \sim 4 (similar pH in our system), the alginate–chitosan complexes obtained from 2% w/v alginate–2% w/v chitosan have $G' \sim 100$ Pa.²⁴ Since we have considered 1% w/v alginate and chitosan, our modulus values were slightly lower when no salt was added. Additionally, the change in G' with salt addition can be utilized to tune the modulus of PECs, which is important for different applications.

As discussed above and widely reported in the literature, the formation of the extrinsic ion pairs with the addition of salt can lead to increased mobility of the polymer chains (plasticization effects).^{45,57,60} On the contrary, free salt ions with bound water in their hydration shells can restrict the mobility of the polymer chains (stiffening effects).⁶¹ These opposing influences of salts in PECs can cause both stiffening and plasticizing effects, as observed in our system. A distinct salt-stiffening behavior has also been reported in a PEC system formed from PVBtMA and PSS.¹³

The PECs were also subjected to increasing strain amplitude from a linear to nonlinear regime, and Figure 5a displays G' as a function of strain amplitude. An increase in G' with salt concentration was similar to that captured in frequency sweep experiments. Beyond the linear viscoelastic region (LVE), a decrease in G' was observed for all samples. The LVE region extended to the higher strain value with salt added. For example, the deviation from the LVE region was observed at 1% strain for $c < 1.0$ M, whereas the LVE region extended to 2.5% for $c = 2$ M, which did not change significantly for c equal to 4 and 6 M.

Characterizing nonlinear viscoelastic response provides additional information regarding the microstructure and is also necessary to understand how samples behave in many applications.^{62,63} In the nonlinear regime, the Lissajous curves (shear stress vs strain) are not elliptical but distorted. The results for $c = 1.0$ M salt concentration with increasing strain are shown in Figure 5b. Chebyshev coefficients were obtained from LAOS data using MITlaos software. Here, the first-order

coefficients e_1 and ν_1 are G' and G'' , respectively. The third-order parameters, e_3 and ν_3 , can be used to hypothesize whether a sample is strain-stiffening ($e_3 > 0$) or strain-softening ($e_3 < 0$) and shear-thickening ($\nu_3 > 0$) or shear-thinning ($\nu_3 < 0$).³⁹ The magnitude of the ratio between the third and first harmonic Chebyshev coefficients, i.e., e_3/e_1 and ν_3/ν_1 , characterizes the nonlinearity in the sample as the higher magnitude indicates increasing nonlinearity.^{63,64} In our experiments, the highest strain amplitude considered was 50%, and the corresponding Lissajous curves for all salt concentrations are shown in Figure 6. Here, the Lissajous curves were more distorted for low salt concentration, in which the LVE region was smaller.

Third-order Chebyshev coefficients for the complexes obtained at different salt concentrations were determined using MITlaos software.³⁹ Table 1 shows the elastic and

Table 1. Chebyshev Coefficients at Selected Strain Rates, Near Nonlinearity, $\gamma_0 = 1.6\%$ for $c = 0.5$ and 1.0 M and $\gamma_0 = 5\%$ for $c = 2.0, 4.0,$ and 6.0 M

salt concentration (M) (near nonlinearity)	e_1	e_3	ν_1	ν_3
0.5	680	5.4	23	−0.5
1.0	2043	7.8	52	−0.5
2.0	11493	36.7	315	−1.1
4.0	7876	21.8	203	−0.1
6.0	5041	26.1	136	−0.4

viscous Chebyshev coefficients measured slightly away from the onset of nonlinearity ($\gamma_0 = 1.6\%$ for $c = 0.5$ and 1.0 M and $\gamma_0 = 5\%$ for $c = 2.0, 4.0,$ and 6.0 M). Note that the strain values are chosen such that they are equidistant from the onset of nonlinearity. Table 2 shows the values determined at the highest measured strain ($\gamma_0 = 50\%$) for all salt concentrations. Here, $e_3 > 0$, and $\nu_3 < 0$ at any salt concentration. These signify the intra-cycle elastic strain stiffening and viscous shear thinning behavior of the sample. An increase in e_3 was observed beyond the onset of the nonlinear regime, such as at the highest measured strain value ($\gamma_0 = 50\%$) considered here.

Table 2. Chebyshev Coefficients and Nonlinear Intensity Ratio at $\gamma_0 = 50\%$

salt concentration (M)	e_1	e_3	ν_1	ν_3	e_3/e_1	ν_3/ν_1
0.5	77	13.4	9	-2.8	0.0078	-0.0210
1.0	286	25.6	25	-5.4	0.0038	-0.0094
2.0	3131	119.7	289	-7.0	0.0032	-0.0033
4.0	2049	85.3	159	-3.2	0.0028	-0.00055
6.0	1239	51.8	105	-2.4	0.0052	-0.0025

Elastic strain stiffening of the PECs can happen due to the stretching of the polymer chains, either of the individual chain or the paired alginate–chitosan chains. The shear thinning can take place likely due to the change of microstructure with applied strain as the chains and complexes do not have any permanent crosslinks or do not have sufficient chain entanglements.^{65,66} This kind of behavior was previously reported for biopolymer gels and filled elastomer, but not for PECs.^{67,68}

LAOS tests were also performed with increasing frequency and strain amplitude to understand the effects of frequency on the nonlinear behavior of the PECs. The stress–strain response over a frequency range of 1–15 rad/s and a strain amplitude range of 1–200% are placed in Pipkin space, as shown in Figure 7.^{63,69,70} G' and e_3 values are also provided for

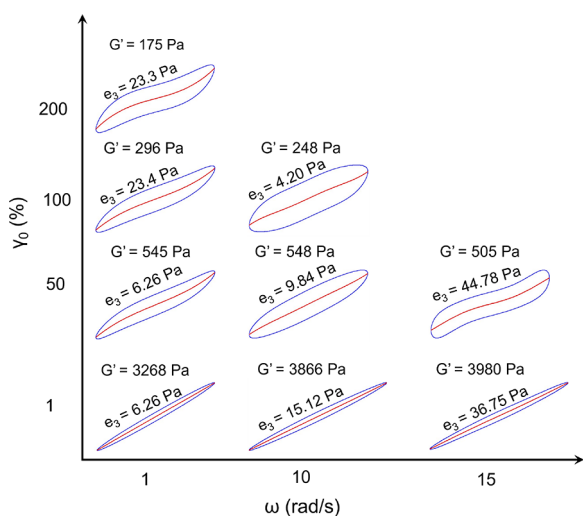


Figure 7. Lissajous curves as a function of frequency and strain (%) for the sample with 1.0 M NaCl. Red dashed lines represent the elastic response of the sample.

each curve. For the strain amplitude of 1%, the response was elliptical with mostly linear elastic contributions. The sample displayed increased plastic behavior with the increase in strain amplitude and frequency, as shown by the increased hysteresis of the Lissajous curves. For example, comparing Lissajous curves for 1 and 10 rad/s, at 100% strain, the hysteresis increased with frequency.

Structural Analysis Using SAXS. To investigate the structure of PECs, SAXS data are collected for samples with different NaCl concentrations and the corresponding $I(q)$ vs q are shown in Figure 8a. No correlation peak in the scattering profile (Figure 8a) was observed. A correlation peak for polyelectrolyte samples, including individual alginate and chitosan solutions, has been reported in the literature.^{32,71}

The broad peak, referred to as the polyelectrolyte peak, is caused by the repulsive electrostatic interactions of polyelectrolytes in solution.⁷² This peak can shift to higher wave vectors with an increase in polymer concentration^{72,73} or can disappear with the addition of salt due to the screening of electrostatic interactions.^{72–75} Molecular dynamics simulations performed on chondroitin sulfate and hyaluronic acid have shown that the polyelectrolyte peaks can disappear due to the long-range and short-range interchain interactions.⁷⁵

SAXS studies on our PECs showed no distinct peaks even when no salt was added. It has been shown in the literature that the polyelectrolyte peak originally present in individual poly(L-lysine hydrochloride) and poly(L-glutamic acid sodium salt) diminished when the complex formed.¹⁷ Similarly, we hypothesize that the electrostatic interactions between alginate and chitosan, resulting in the alginate–chitosan complexes, have led to the disappearance of the polyelectrolyte peaks in our system.

For the undoped sample, two power law regions with different slopes can be identified (Figure 8 and Figure S5). Hence, the scattering data were fit with two power law models in a piecewise fashion as

$$I(q) = \begin{cases} \frac{A}{q^{-m_1}} & \text{for } q \leq q_c \\ A \cdot \frac{q_c^{-m_1}}{q_c^{-m_2}} \frac{1}{q^{-m_2}} & \text{for } q \geq q_c \end{cases}$$

where q_c captures the cross-over from one slope to another. For the lower q region, scaling A sets the overall intensity and scaling for the second power law region ($A \cdot \frac{q_c^{-m_1}}{q_c^{-m_2}}$) is scaled to match the first. At $q > q_c$ ($\sim 0.0143 \text{ \AA}^{-1}$), complexes exhibited a $I(q) \sim q^{-2.2}$ behavior, which can be attributed to the structure formation upon complexation of alginate and chitosan with mass fractal dimension of 2.2.^{13,17} At $q < q_c$, a $I(q) \sim q^{-4.4}$ behavior was observed, which indicates the formation of larger aggregates of such polyelectrolyte complexes.^{13,17}

The scattering profile for the doped sample was different from those obtained for the undoped samples. In doped samples for $c = 0.1$ and 0.5 M, upturns were noticed in the $q < 0.015$ followed by broad shoulder-like scattering features in $0.015 < q < 0.1 \text{ \AA}^{-1}$. For samples with a salt concentration between 1.0 to 6.0 M, upturns were noticed in the $q < 0.009 \text{ \AA}^{-1}$, while broad shoulder-like scattering features were seen in $0.009 < q < 0.1 \text{ \AA}^{-1}$, where the scattering profiles were similar and showed only different absolute intensities. If the shoulder-like scattering observed in the high- q region is associated with the conformation of the complexes (assumed to be semirigid worm-like chain conformation), the low- q upturn is with the aggregation of such complexes. On the other hand, the scattering plateaus seen in the $0.1 < q < 0.6 \text{ \AA}^{-1}$ are associated with the incoherent (background) scattering where the scattering intensity increases with increasing salt.

The similarity in the shoulder-like scattering indicates that the chain conformations (structure) are not significantly different. An increase in scattering intensity was observed up to $c = 2.0$ M, and a further increase in salt concentration showed a slight decrease in intensity. We hypothesize that PECs for c up to 2.0 M have a more defined polymer-rich phase due to the osmotic ejection of water from PECs. The

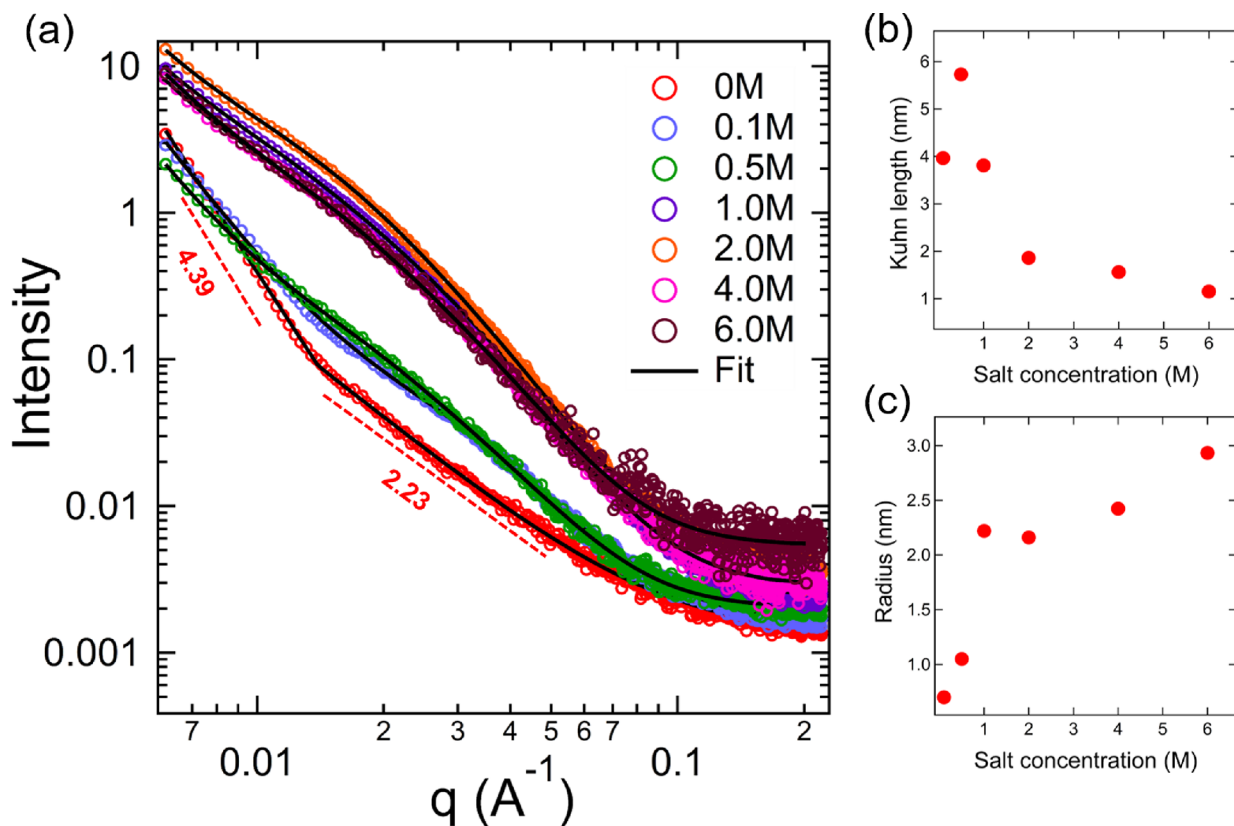


Figure 8. Scattering data from SAXS experiments: (a) scattering intensity as a function of q . Parameters obtained from the fitting using the WLC model: (b) Kuhn length and (c) cylinder radius as a function of salt concentration.

ejection of water increases the polymer concentration and hence electron density contrast between the polymer-rich phase and solvent, leading to the increased intensity. This agrees with the observation from the phase diagram, which displayed a decrease in polymer concentration when the added $c > 2.0$ M. Similarly, rheological tests also displayed an increase in shear modulus when $c < 2.0$ M, and the modulus was decreased with a further increase in salt.

A combined power-law and worm-like chain (WLC) model was used to fit the data for the doped samples (Figure 8 and Figure S6).^{76,77} Similar to many biological samples, the application of the WLC model that considers a semiflexible (or semirigid) polymer chain is appropriate here.^{71,78} Power-law model captures the low- q upturn in SAXS curves, and the WLC model captures the subsequent q range associated with the chain conformation of the semirigid (semiflexible) polyelectrolytes.

The scattering of semiflexible chain with excluded volume effects with Kuhn length (b), contour length (L), and polydisperse radius (R) is given by⁷⁶

$$I(q, L, b, R) = f_s S(q, L, b) P(q, R)$$

where f_s is a scaling factor, $S(q, L, b)$ is the scattering function of a single semiflexible chain with excluded volume effects and $P(q, R)$ is the scattering function of the rigid rod (alginate and chitosan associated structure) of radius, R .

$$P(q, R) = \left[\frac{2J_1(qR)}{qR} \right]^2$$

$S(q, L, b)$ is given by

$$S(q, L, b) = S_{\text{exv}}(q, L, b) + C \left(\frac{L}{b} \right) \left[\frac{4}{15} + \frac{7}{15u} - \left(\frac{11}{15} + \frac{7}{15u} \right) \exp(-u) \right] \frac{b}{L}$$

where

$$S_{\text{exv}}(q, L, b) = w(qR_g) S_{\text{Debye}}(q, L, b) + [W(qR_g)] [C_1(qR_g)^{-1/\nu}]$$

The Kuhn length and radius obtained from the WLC model fit (Figure S6) are shown in Figure 8b,c. Beyond $c = 0.5$ M, a clear trend of an increase in radius and a decrease in Kuhn length with increasing c can be noticed. These observations further support our hypothesis that doping forms extrinsic ion pairs, which can cause higher local mobility attributed to the increase in chain flexibility, shown by the decrease in Kuhn length, and favor the formation of a “looser ladder”-type association between polyelectrolytes causing an increase in radius.

CONCLUSIONS

In summary, we have reported the salt-driven phase behavior, microstructure, and rheological properties of PECs prepared from two oppositely charged natural polymers, alginate and chitosan. We attempted to understand the salt-induced phase behavior in natural polyelectrolyte systems. The PECs showed two-phase solid–liquid separation at all salt concentrations studied. This behavior is unique compared to the usually seen salt-driven solid-to-liquid transition in synthetic polyelectrolyte

systems. The lack of liquid–liquid phase transition is attributed to the slightly hydrophobic nature of chitosan and resistance to conformational change at high salt concentrations for longer, semiflexible chains. The structure formed by the electrostatic interactions between the oppositely charged alginate and chitosan chains underwent changes due to the addition of salt. The complexes obtained displayed a tunable shear modulus with changing salt concentrations. With increasing salt concentration, the samples displayed a salt-stiffening behavior with an increase in shear modulus, which has been attributed to the loss of water. Beyond a certain limit in the salt concentration, the shear modulus of the complex phase decreased due to the breakage of intrinsic ion pairs formed between the polyelectrolytes. This agrees with the increase in chain flexibility with the addition of salt shown by the value of Kuhn length obtained from SAXS analysis. The results presented here provide insights into the salt-induced complexation phenomenon in natural polyelectrolytes, which can potentially help us elucidate the structure–property relationship of the PECs. Such understanding can be useful for applications of natural PEs in bioprinting, drug delivery, and other applications.

■ ASSOCIATED CONTENT

SI Supporting Information

The Supporting Information is available free of charge at <https://pubs.acs.org/doi/10.1021/acs.biomac.3c00171>.

Kraemer plot of inherent viscosity vs concentration; table showing Mark–Houwink constants and estimated molecular weights for alginate and chitosan; FTIR spectra and %DD estimation for chitosan; images showing phase separation using different salts; $\tan \delta$ for the complex phase with different NaCl concentrations; SAXS fitting for doped and undoped samples (PDF)

■ AUTHOR INFORMATION

Corresponding Author

Santanu Kundu – Dave C. Swalm School of Chemical Engineering, Mississippi State University, Mississippi State, Mississippi 39762, United States; orcid.org/0000-0002-0767-0512; Email: santanukundu@che.msstate.edu

Authors

Anandavalli Varadarajan – Dave C. Swalm School of Chemical Engineering, Mississippi State University, Mississippi State, Mississippi 39762, United States

Logan T. Kearney – Chemical Sciences Division, Oak Ridge National Laboratory, Oak Ridge, Tennessee 37831, United States

Jong K. Keum – Neutron Scattering Science Division and Center for Nanophase Materials Sciences, Oak Ridge National Laboratory, Oak Ridge, Tennessee 37831, United States

Amit K Naskar – Chemical Sciences Division, Oak Ridge National Laboratory, Oak Ridge, Tennessee 37831, United States; orcid.org/0000-0002-1094-0325

Complete contact information is available at: <https://pubs.acs.org/doi/10.1021/acs.biomac.3c00171>

Author Contributions

A.V. and S.K. designed the experiments and conducted data analysis and interpretation. A.V. conducted the experiments. S.K. conceptualized and oversaw the research. L.T.K., J.K.K., and A.K.N. performed the SAXS experiments and analyzed the data. The manuscript was written by A.V. and S.K. and included feedback from all authors. All authors have approved the final version of the manuscript.

Funding

A.V. and S.K. would like to acknowledge funding support from the National Science Foundation [DMR-2004501]. L.T.K. and A.K.N. acknowledge support from the US Department of Energy, Office of Science, Basic Energy Sciences, Materials Sciences and Engineering Division [FWP# ERKCK60] for SAXS data collection with polyelectrolyte complexes. The SAXS facility has been developed at the Oak Ridge National Laboratory (ORNL) under the Laboratory Directed Research and Development Program. J.K.K. used the resource of Center for Nanophase Materials Sciences (CNMS), which is a US Department of Energy, Office of Science User Facility at ORNL.

Notes

The authors declare no competing financial interest.

■ REFERENCES

- (1) Dobrynin, A. V.; Rubinstein, M. Theory of Polyelectrolytes in Solutions and at Surfaces. *Prog. Polym. Sci.* **2005**, *30*, 1049–1118.
- (2) Cazorla-Luna, R.; Martín-Illana, A.; Notario-Pérez, F.; Ruiz-Caro, R.; Veiga, M.-D. Naturally Occurring Polyelectrolytes and Their Use for the Development of Complex-Based Mucoadhesive Drug Delivery Systems: An Overview. *Polymer* **2021**, *13*, 2241.
- (3) Schanze, K. S.; Shelton, A. H. Functional Polyelectrolytes. *Langmuir* **2009**, *25*, 13698–13702.
- (4) Meka, V. S.; Sing, M. K. G.; Pichika, M. R.; Nali, S. R.; Kolapalli, V. R. M.; Kesharwani, P. A Comprehensive Review on Polyelectrolyte Complexes. *Drug Discovery Today* **2017**, *22*, 1697–1706.
- (5) Moschakis, T.; Biliaderis, C. G. Biopolymer-Based Coacervates: Structures, Functionality and Applications in Food Products. *Curr. Opin. Colloid Interface Sci.* **2017**, *28*, 96–109.
- (6) Black, K. A.; Priftis, D.; Perry, S. L.; Yip, J.; Byun, W. Y.; Tirrell, M. Protein Encapsulation via Polypeptide Complex Coacervation. *ACS Macro Lett.* **2014**, *3*, 1088–1091.
- (7) Liu, Y.; Momani, B.; Winter, H. H.; Perry, S. L. Rheological Characterization of Liquid-to-Solid Transitions in Bulk Polyelectrolyte Complexes. *Soft Matter* **2017**, *13*, 7332–7340.
- (8) Liu, Y.; Winter, H. H.; Perry, S. L. Linear Viscoelasticity of Complex Coacervates. *Adv. Colloid Interface Sci.* **2017**, *239*, 46–60.
- (9) Chollakup, R.; Smitthipong, W.; Eisenbach, C. D.; Tirrell, M. Phase Behavior and Coacervation of Aqueous Poly(Acrylic Acid)–Poly(Allylamine) Solutions. *Macromolecules* **2010**, *43*, 2518–2528.
- (10) Wang, Q.; Schlenoff, J. B. The Polyelectrolyte Complex/Coacervate Continuum. *Macromolecules* **2014**, *47*, 3108–3116.
- (11) Jha, P. K.; Desai, P. S.; Li, J.; Larson, R. G. PH and Salt Effects on the Associative Phase Separation of Oppositely Charged Polyelectrolytes. *Polymer* **2014**, *6*, 1414–1436.
- (12) Perry, S. L.; Li, Y.; Priftis, D.; Leon, L.; Tirrell, M. The Effect of Salt on the Complex Coacervation of Vinyl Polyelectrolytes. *Polymer* **2014**, *6*, 1756–1772.
- (13) Meng, S.; Ting, J. M.; Wu, H.; Tirrell, M. V. Solid-to-Liquid Phase Transition in Polyelectrolyte Complexes. *Macromolecules* **2020**, *53*, 7944–7953.
- (14) Nguyen, M.; Sherck, N.; Shen, K.; Edwards, C. E. R.; Yoo, B.; Köhler, S.; Speros, J. C.; Helgeson, M. E.; Delaney, K. T.; Shell, M. S.; Fredrickson, G. H. Predicting Polyelectrolyte Coacervation from a Molecularly Informed Field-Theoretic Model. *Macromolecules* **2022**, *55*, 9868–9879.

- (15) Fares, H. M.; Ghossoub, Y. E.; Delgado, J. D.; Fu, J.; Urban, V. S.; Schlenoff, J. B. Scattering Neutrons along the Polyelectrolyte Complex/Coacervate Continuum. *Macromolecules* **2018**, *51*, 4945–4955.
- (16) Spruijt, E.; Leermakers, F. A. M.; Fokkink, R.; Schweins, R.; van Well, A. A.; Cohen Stuart, M. A.; van der Gucht, J. Structure and Dynamics of Polyelectrolyte Complex Coacervates Studied by Scattering of Neutrons, X-Rays, and Light. *Macromolecules* **2013**, *46*, 4596–4605.
- (17) Marciel, A. B.; Srivastava, S.; Tirrell, M. V. Structure and Rheology of Polyelectrolyte Complex Coacervates. *Soft Matter* **2018**, *14*, 2454–2464.
- (18) Schmitt, C.; Turgeon, S. L. Protein/Polysaccharide Complexes and Coacervates in Food Systems. *Adv. Colloid Interface Sci.* **2011**, *167*, 63–70.
- (19) Moss, J. M.; Van Damme, M.-P. I.; Murphy, W. H.; Preston, B. N. Dependence of Salt Concentration on Glycosaminoglycan–Lysozyme Interactions in Cartilage. *Arch. Biochem. Biophys.* **1997**, *348*, 49–55.
- (20) Seyrek, E.; Dubin, P. L.; Henriksen, J. Nonspecific electrostatic binding characteristics of the heparin-antithrombin interaction. *Biopolymers* **2007**, *86*, 249–259.
- (21) Zhao, H.; Sun, C.; Stewart, R. J.; Waite, J. H. Cement Proteins of the Tube-Building Polychaete *Phragmatopoma Californica*. *J. Biol. Chem.* **2005**, *280*, 42938–42944.
- (22) Lalevée, G.; David, L.; Montembault, A.; Blanchard, K.; Meadows, J.; Malaise, S.; Crépet, A.; Grillo, I.; Morfin, I.; Delair, T.; Sudre, G. Highly Stretchable Hydrogels from Complex Coacervation of Natural Polyelectrolytes. *Soft Matter* **2017**, *13*, 6594–6605.
- (23) Shi, X.; Du, Y.; Sun, L.; Zhang, B.; Dou, A. Polyelectrolyte Complex Beads Composed of Water-Soluble Chitosan/Alginate: Characterization and Their Protein Release Behavior. *J. Appl. Polym. Sci.* **2006**, *100*, 4614–4622.
- (24) Afzal, S.; Maswal, M.; Dar, A. A. Rheological Behavior of PH Responsive Composite Hydrogels of Chitosan and Alginate: Characterization and Its Use in Encapsulation of Citral. *Colloids Surf., B* **2018**, *169*, 99–106.
- (25) Baruch, L.; Machluf, M. Alginate–Chitosan Complex Coacervation for Cell Encapsulation: Effect on Mechanical Properties and on Long-Term Viability. *Biopolymers* **2006**, *82*, 570–579.
- (26) Kim, H.-J.; Lee, H.-C.; Oh, J.-S.; Shin, B.-A.; Oh, C.-S.; Park, R.-D.; Yang, K.-S.; Cho, C.-S. Polyelectrolyte Complex Composed of Chitosan and Sodium Alginate for Wound Dressing Application. *J. Biomater. Sci., Polym. Ed.* **1999**, *10*, 543–556.
- (27) Meng, X.; Tian, F.; Yang, J.; He, C.-N.; Xing, N.; Li, F. Chitosan and Alginate Polyelectrolyte Complex Membranes and Their Properties for Wound Dressing Application. *J. Mater. Sci.: Mater. Med.* **2010**, *21*, 1751–1759.
- (28) Hashemnejad, S. M.; Kundu, S. Strain Stiffening and Negative Normal Stress in Alginate Hydrogels. *J. Polym. Sci., Part B: Polym. Phys.* **2016**, *54*, 1767–1775.
- (29) Hashemnejad, S. M.; Kundu, S. Rheological Properties and Failure of Alginate Hydrogels with Ionic and Covalent Crosslinks. *Soft Matter* **2019**, *15*, 7852–7862.
- (30) Lee, K. Y.; Mooney, D. J. Alginate: Properties and Biomedical Applications. *Prog. Polym. Sci.* **2012**, *37*, 106–126.
- (31) Knaul, J. Z.; Kasaai, M. R.; Bui, V. T.; Creber, K. A. M. Characterization of Deacetylated Chitosan and Chitosan Molecular Weight Review. *Can. J. Chem.* **1998**, *76*, 1699–1706.
- (32) Boucard, N.; David, L.; Rochas, C.; Montembault, A.; Viton, C.; Domard, A. Polyelectrolyte Microstructure in Chitosan Aqueous and Alcohol Solutions. *Biomacromolecules* **2007**, *8*, 1209–1217.
- (33) Yilmaz, T.; Maldonado, L.; Turasan, H.; Kokini, J. Thermodynamic Mechanism of Particulation of Sodium Alginate and Chitosan Polyelectrolyte Complexes as a Function of Charge Ratio and Order of Addition. *J. Food Eng.* **2019**, *254*, 42–50.
- (34) Nalini, T.; Basha, S. K.; Mohamed Sadiq, A. M.; Kumari, V. S.; Kaviyarasu, K. Development and Characterization of Alginate / Chitosan Nanoparticulate System for Hydrophobic Drug Encapsulation. *J. Drug Delivery Sci. Technol.* **2019**, *52*, 65–72.
- (35) Phoeung, T.; Spanedda, M. V.; Roger, E.; Heurtault, B.; Fournel, S.; Reisch, A.; Mutschler, A.; Perrin-Schmitt, F.; Hemmerlé, J.; Collin, D.; Rawiso, M.; Boulmedais, F.; Schaaf, P.; Lavalle, P.; Frisch, B. Alginate/Chitosan Compact Polyelectrolyte Complexes: A Cell and Bacterial Repellent Material. *Chem. Mater.* **2017**, *29*, 10418–10425.
- (36) Costa, R. R.; Costa, A. M. S.; Caridade, S. G.; Mano, J. F. Compact Saloplastic Membranes of Natural Polysaccharides for Soft Tissue Engineering. *Chem. Mater.* **2015**, *27*, 7490–7502.
- (37) Costalat, M.; Alcouffe, P.; David, L.; Delair, T. Controlling the Complexation of Polysaccharides into Multi-Functional Colloidal Assemblies for Nanomedicine. *J. Colloid Interface Sci.* **2014**, *430*, 147–156.
- (38) Costalat, M.; Alcouffe, P.; David, L.; Delair, T. Macro-Hydrogels versus Nanoparticles by the Controlled Assembly of Polysaccharides. *Carbohydr. Polym.* **2015**, *134*, 541–546.
- (39) Ewoldt, R. H.; Hosoi, A. E.; McKinley, G. H. New Measures for Characterizing Nonlinear Viscoelasticity in Large Amplitude Oscillatory Shear. *J. Rheol.* **2008**, *52*, 1427–1458.
- (40) Rinaudo, M. On the Abnormal Exponents λ_V and λ_D in Mark Houwink Type Equations for Worm-like Chain Polysaccharides. *Polym. Bull.* **1992**, *27*, 585–589.
- (41) Kasaai, M. R. Calculation of Mark–Houwink–Sakurada (MHS) Equation Viscometric Constants for Chitosan in Any Solvent–Temperature System Using Experimental Reported Viscometric Constants Data. *Carbohydr. Polym.* **2007**, *68*, 477–488.
- (42) Kasaai, M. R. Determination of the Degree of N-Acetylation for Chitin and Chitosan by Various NMR Spectroscopy Techniques: A Review. *Carbohydr. Polym.* **2010**, *79*, 801–810.
- (43) Moore, G. K.; Roberts, G. A. F. Determination of the Degree of N-Acetylation of Chitosan. *Int. J. Biol. Macromol.* **1980**, *2*, 115–116.
- (44) Kasaai, M. R. A Review of Several Reported Procedures to Determine the Degree of N-Acetylation for Chitin and Chitosan Using Infrared Spectroscopy. *Carbohydr. Polym.* **2008**, *71*, 497–508.
- (45) Shamoun, R. F.; Reisch, A.; Schlenoff, J. B. Extruded Saloplastic Polyelectrolyte Complexes. *Adv. Funct. Mater.* **2012**, *22*, 1923–1931.
- (46) Li, L.; Rumyantsev, A. M.; Srivastava, S.; Meng, S.; de Pablo, J. J.; Tirrell, M. V. Effect of Solvent Quality on the Phase Behavior of Polyelectrolyte Complexes. *Macromolecules* **2021**, *54*, 105–114.
- (47) Ghasemi, M.; Larson, R. G. Future Directions in Physicochemical Modeling of the Thermodynamics of Polyelectrolyte Coacervates. *AIChE J.* **2022**, *68*, No. e17646.
- (48) Li, L.; Srivastava, S.; Andreev, M.; Marciel, A. B.; de Pablo, J. J.; Tirrell, M. V. Phase Behavior and Salt Partitioning in Polyelectrolyte Complex Coacervates. *Macromolecules* **2018**, *51*, 2988–2995.
- (49) Rabelo, R. S.; Tavares, G. M.; Prata, A. S.; Hubinger, M. D. Complexation of Chitosan with Gum Arabic, Sodium Alginate and κ -Carrageenan: Effects of PH, Polymer Ratio and Salt Concentration. *Carbohydr. Polym.* **2019**, *223*, No. 115120.
- (50) Carneiro-da-Cunha, M. G.; Cerqueira, M. A.; Souza, B. W. S.; Teixeira, J. A.; Vicente, A. A. Influence of Concentration, Ionic Strength and PH on Zeta Potential and Mean Hydrodynamic Diameter of Edible Polysaccharide Solutions Envisaged for Multilayered Films Production. *Carbohydr. Polym.* **2011**, *85*, 522–528.
- (51) Fu, J.; Fares, H. M.; Schlenoff, J. B. Ion-Pairing Strength in Polyelectrolyte Complexes. *Macromolecules* **2017**, *50*, 1066–1074.
- (52) Geoghegan, M. The Swelling of Weak Polyelectrolytes at Low Salt Concentrations in Dilute Solution. *Polymer* **2017**, *112*, 414–417.
- (53) Zhang, J.; Kou, R.; Liu, G. Effect of Salt Concentration on the PH Responses of Strong and Weak Polyelectrolyte Brushes. *Langmuir* **2017**, *33*, 6838–6845.
- (54) Overbeek, J. T. G.; Voorn, M. J. Phase Separation in Polyelectrolyte Solutions. Theory of Complex Coacervation. *J. Cell. Comp. Physiol.* **1957**, *49*, 7–26.
- (55) Ghostine, R. A.; Shamoun, R. F.; Schlenoff, J. B. Doping and Diffusion in an Extruded Saloplastic Polyelectrolyte Complex. *Macromolecules* **2013**, *46*, 4089–4094.

- (56) Dautzenberg, H.; Kriz, J. Response of Polyelectrolyte Complexes to Subsequent Addition of Salts with Different Cations. *Langmuir* **2003**, *19*, 5204–5211.
- (57) Yang, M.; Digby, Z. A.; Schlenoff, J. B. Precision Doping of Polyelectrolyte Complexes: Insight on the Role of Ions. *Macromolecules* **2020**, *53*, 5465–5474.
- (58) Schlenoff, J. B.; Yang, M.; Digby, Z. A.; Wang, Q. Ion Content of Polyelectrolyte Complex Coacervates and the Donnan Equilibrium. *Macromolecules* **2019**, *52*, 9149–9159.
- (59) Spruijt, E.; Cohen Stuart, M. A.; van der Gucht, J. Linear Viscoelasticity of Polyelectrolyte Complex Coacervates. *Macromolecules* **2013**, *46*, 1633–1641.
- (60) Porcel, C. H.; Schlenoff, J. B. Compact Polyelectrolyte Complexes: "Saloplastic" Candidates for Biomaterials. *Biomacromolecules* **2009**, *10*, 2968–2975.
- (61) Zhang, R.; Zhang, Y.; Antila, H. S.; Lutkenhaus, J. L.; Sammalkorpi, M. Role of Salt and Water in the Plasticization of PDAC/PSS Polyelectrolyte Assemblies. *J. Phys. Chem. B* **2017**, *121*, 322–333.
- (62) Hyun, K.; Wilhelm, M.; Klein, C. O.; Cho, K. S.; Nam, J. G.; Ahn, K. H.; Lee, S. J.; Ewoldt, R. H.; McKinley, G. H. A Review of Nonlinear Oscillatory Shear Tests: Analysis and Application of Large Amplitude Oscillatory Shear (LAOS). *Prog. Polym. Sci.* **2011**, *36*, 1697–1753.
- (63) Hashemnejad, S. M.; Kundu, S. Nonlinear Elasticity and Cavitation of a Triblock Copolymer Gel. *Soft Matter* **2015**, *11*, 4315–4325.
- (64) Kőcuti, Z.; Völker-Pop, L.; Brandstätter, M.; Kokavec, J.; Ailer, P.; Palkovics, L.; Szabó, G.; Czirják, A. Exploring the Nonlinear Viscoelasticity of a High Viscosity Silicone Oil with Laos. *Appl. Rheol.* **2016**, *26*, 1–9.
- (65) Carmona, J. A.; Ramírez, P.; Calero, N.; Muñoz, J. Large Amplitude Oscillatory Shear of Xanthan Gum Solutions. Effect of Sodium Chloride (NaCl) Concentration. *J. Food Eng.* **2014**, *126*, 165–172.
- (66) Duvarci, O. C.; Yazar, G.; Kokini, J. L. The Comparison of LAOS Behavior of Structured Food Materials (Suspensions, Emulsions and Elastic Networks). *Trends Food Sci. Technol.* **2017**, *60*, 2–11.
- (67) Papon, A.; Montes, H.; Lequeux, F.; Guy, L. Nonlinear Rheology of Model Filled Elastomers. *J. Polym. Sci., Part B: Polym. Phys.* **2010**, *48*, 2490–2496.
- (68) Goudoulas, T. B.; Germann, N. Phase Transition Kinetics and Rheology of Gelatin-Alginate Mixtures. *Food Hydrocolloids* **2017**, *66*, 49–60.
- (69) Mishra, S.; Badani Prado, R. M.; Kundu, S. Concentration-Dependent Mechanical Behavior of Physically Assembled Triblock Copolymer Gels. *ACS Appl. Polym. Mater.* **2020**, *2*, 5388–5397.
- (70) Mishra, S.; Prado, R. M. B.; Lacy, T. E.; Kundu, S. Investigation of Failure Behavior of a Thermoplastic Elastomer Gel. *Soft Matter* **2018**, *14*, 7958–7969.
- (71) Josef, E.; Bianco-Peled, H. Conformation of a Natural Polyelectrolyte in Semidilute Solutions with No Added Salt. *Soft Matter* **2012**, *8*, 9156–9165.
- (72) Lalevé, G.; Sudre, G.; Montembault, A.; Meadows, J.; Malaise, S.; Crépet, A.; David, L.; Delair, T. Polyelectrolyte Complexes via Desalting Mixtures of Hyaluronic Acid and Chitosan—Physicochemical Study and Structural Analysis. *Carbohydr. Polym.* **2016**, *154*, 86–95.
- (73) Yethiraj, A.; Shew, C.-Y. Structure of Polyelectrolyte Solutions. *Phys. Rev. Lett.* **1996**, *77*, 3937–3940.
- (74) Prabhu, V. M.; Amis, E. J.; Bossev, D. P.; Rosov, N. Counterion Associative Behavior with Flexible Polyelectrolytes. *J. Chem. Phys.* **2004**, *121*, 4424–4429.
- (75) Chremos, A.; Horkay, F. Disappearance of the Polyelectrolyte Peak in Salt-Free Solutions. *Phys. Rev. E* **2020**, *102*, No. 012611.
- (76) Shao, M.; Keum, J. K.; Kumar, R.; Chen, J.; Browning, J. F.; Das, S.; Chen, W.; Hou, J.; Do, C.; Littrell, K. C.; Rondinone, A.; Geoghegan, D. B.; Sumpster, B. G.; Xiao, K. Understanding How Processing Additives Tune the Nanoscale Morphology of High Efficiency Organic Photovoltaic Blends: From Casting Solution to Spin-Cast Thin Film. *Adv. Funct. Mater.* **2014**, *24*, 6647–6657.
- (77) Das, S.; Keum, J. K.; Browning, J. F.; Gu, G.; Yang, B.; Dyck, O.; Do, C.; Chen, W.; Chen, J.; Ivanov, I. N.; Hong, K.; Rondinone, A. J.; Joshi, P. C.; Geoghegan, D. B.; Duscher, G.; Xiao, K. Correlating High Power Conversion Efficiency of PTB7:PC71BM Inverted Organic Solar Cells with Nanoscale Structures. *Nanoscale* **2015**, *7*, 15576–15583.
- (78) Kratky, O.; Porod, G. Röntgenuntersuchung Gelöster Fadenmoleküle. *Recl. Trav. Chim. Pays-Bas* **1949**, *68*, 1106–1122.